Research Article

Obulesu Mopuri, Charankumar Ganteda, Sarah A. Alsalhi, Sami Ullah Khan, Aruna Ganjikunta, Vediyappan Govindan*, Faris Alqurashi, and Mohamed Kchaou

Inclined surface mixed convection flow of viscous fluid with porous medium and Soret effects

https://doi.org/10.1515/phys-2023-0209
received December 30, 2023; accepted February 20, 2024

Abstract: The combined heat and mass transfer phenomenon is a significant aspect of engineering and industrial processes. This phenomenon finds applications in various areas such as air conditioning, cooling and heating control of electronic devices, reactors, chemical systems, and emission processes. This research model focuses on the analysis of mixed convection flow of a viscous fluid with heat and mass transfer on an inclined surface with porous medium characteristics. The study also considers external heat transfer effects, radiation, Soret influence, and chemical reactions. A perturbation solution is derived in closed form, and the impact of various parameters on the thermal behavior is investigated. A comparative analysis of the heating and cooling regimes in plate flow is conducted, revealing a reduction in velocity in the heated plate regime with changes in the permeability parameter and an increase in concentration phase due to the Soret number.

*** Corresponding author: Vediyappan Govindan,** Department of Mathematics, Hindustan Institute of Technology and Science, Chennai, India, e-mail: govindoviya@gmail.com
Obulesu Mopuri: Department of Mathematics, Ramireddy Subbarami Reddy Engineering College (Autonomous) Kadanuthala, 524142, S.P.S.R. Nellore (Dist), Andhra Pradesh, India
Charankumar Ganteda: Department of Engineering Mathematics, College of Engineering, Koneru Lakshmaiah Education Foundation, Vaddeswaram, AP-522 302, India
Sarah A. Alsalhi: Department of Physics, College of Science, Princess Nourah bint Abdulrahman University, P.O. Box 84428, Riyadh, 11671, Saudi Arabia
Sami Ullah Khan: Department of Mathematics, Namal University, Mianwali, 42250, Pakistan
Aruna Ganjikunta: Department of Mathematics, GITAM University, Hyderabad, 502329, Telangana, India
Faris Alqurashi: Department of Mechanical Engineering, College of Engineering, University of Bisha, P.O. Box 001, Bisha, Saudi Arabia, e-mail: fars421@hotmail.com
Mohamed Kchaou: Department of Mechanical Engineering, College of Engineering, University of Bisha, P.O. Box 001, Bisha, Saudi Arabia, e-mail: kchaou.mohamed@yahoo.fr

Keywords: mixed convection flow, porous medium, Soret effects, thermal radiation, perturbation solution

Nomenclature

B_0	magnetic field strength
C'	fluid concentration
C_p	specific heat
C'_∞	ambient concentration
D	mass diffusivity
E	Eckert number
F	radiation parameter
Gr	Grashof number
g	gravity
K	permeability parameter
k	thermal conductivity
K_C	reaction coefficient
K_P	permeability of porous space
K_0	chemical reaction parameter
M	magnetic parameter
Pr	Prandtl number
Q	heat sink
Q_1	external heat source
q'_r	radiative heat flux
S_0	Soret parameter
Sc	Schmidt number
T'	fluid temperature
T'_∞	ambient temperature
(u', v')	velocity components
ϑ	kinematic viscosity
α	inclined angle
σ	electric conductivity
ρ	density

1 Introduction

The magneto-hydro-dynamics (MHD) phenomenon is significant in plasma physics, with various applications in industrial and engineering processes. In cases of electrically conducting flow, MHD characteristics arise when magnetic forces act on the fluid flow. Important applications of MHD flows include cooling nuclear reactors, enhancing geothermal reservoirs, providing thermal protection, aiding in oil recovery, and facilitating packed-bed catalytic processes. Chamkha [1] studied MHD effects in accelerating flow with a heated source. Pal and Mondal [2] presented visualizations of convective phenomena influenced by dynamic MHD effects. Obulesu *et al.* [3] investigated different slip effects in MHD flow. Mahmoud [4] discussed vertically fluctuating surface flow under MHD influence. Turkyilmazoglu [5] analyzed MHD effects on a permeable moving surface with mixed convective transport. Nandalur [6] examined infinite surface flow with MHD phenomena. Khan *et al.* [7] visualized Carreau fluid flow with magnetized impact. Mansour *et al.* [8] examined the impact of MHD on bio-convection in a cavity with a moving surface flow. Kumar *et al.* [9] studied rotating MHD flow using Noumerov's scheme. Lou *et al.* [10] analyzed rotating flow considering the effects of Lorentz force and Coriolis contribution. Ashraf *et al.* [11] discussed tangent hyperbolic flow in nanofluids with MHD applications. Ma *et al.* [12] investigated the flow in micro-tubes with MHD characteristics. Prabhakar Reddy and Jefta Sunzu [13] conducted a thermos-diffusion analysis of MHD-driven flow.

Heat and mass transport play a crucial role in a variety of industrial processes and engineering systems. The significance of understanding heat and mass transport patterns is evident in manufacturing processes, polymer solutions, rolling phenomena, metal casting, cooling processes, and heat transfer, among others. The study of heat transport is particularly important in chemical engineering and other engineering processes. Rashidi *et al.* [14] conducted an analysis of changes in mass and heat transfer influenced by buoyancy-driven flow. Shankar Goud and Dharmendar Reddy [15] investigated the Soret and Dufour effects in infinite plate flow, considering different mass and heat transfer characteristics. Seid *et al.* [16] studied heat and mass transfer in magnetized flow. Rauf *et al.* [17] examined the thermal transport phenomena in hybrid nanofluid flow. Siddique *et al.* [18] reported similar findings for viscoelastic fluids. Additionally, recent developments in fluid flow under various flow assumptions have been discussed in previous studies [19–23]. Previous literature [24–27] discuss various physical applications of highly dispersed transition metal oxide nanoclusters in mesoporous silica, pressure oscillation in low-velocity steam jet condensation, global sensitivity approaches that take into account model and parameter uncertainty, and closed-loop geothermal systems based on net present value. In a study by Bhatti *et al.* [28], the convective flow of Maxwell fluid was deduced using Lie transform analysis.

The current study explores the significance of mixed convection and thermos-diffusion phenomena in viscous fluid flow on an inclined surface. The investigation focuses on the permeability of porous media and the influence of inclined magnetic forces. Additionally, the impact of external heating sources and radiation on thermal transport processes is considered. The study also examines the effects of Soret diffusion and chemical reactions. The analysis involves varying parameters for both the cooler and heated plate, with perturbation simulations conducted to develop a highly accurate model. Physical analysis is presented graphically. Li *et al.* [29–32] recently studied fluid flow behavior under multi-flow assumptions with different boundary conditions and geometries. Yu *et al.* [33], Yang *et al.* [34], and Zhu *et al.* [35] explored hybrid empirical numerical techniques for tubing threaded connections, heat flow in 3D thermal metamaterials, and generalized micro-fluid rectifiers with anisotropic hollow channels. Sun *et al.* [36] and Kong *et al.* [37] investigated the shear-thickening materials and the use of hybrid $CaAl_{12}O_{19}$:Mn^{4+} doped with Ga^{3+} for plant growth lighting.

2 Mathematical formulation

The study is focused on the flow of a viscous fluid over an inclined surface. The fluid is assumed to be incompressible. The flow is induced by the motion of the inclined surface. Figure 1 depicts the schematic flow diagram with coordinate axes. The effects of magnetic force and permeability of the porous medium are taken into account. Let B_0 be the magnetic force strength. Assume u' is the velocity component, T' is the temperature while C' is the concentration. The surface endorsed temperature is T_w, while C_w denotes the plate surface concentration. Furthermore, the ambient concentration and temperature are expressed with C_∞ and T_∞, respectively. In energy equation, the external heating relations and radiative applications are contributed. With such assumptions, the governing equations lead to [3].

$$\frac{\partial v'}{\partial y'} = 0, \tag{1}$$

$$v'\frac{\partial u'}{\partial y'} = \vartheta\frac{\partial^2 u'}{\partial y'^2} + g\beta_T(T' - T'_\infty)\cos\alpha + g\beta_C(C' - C'_\infty)\cos\alpha - \frac{\sigma B_0^2}{\rho}\sin^2\gamma u' - \vartheta\frac{u'}{K_P}, \tag{2}$$

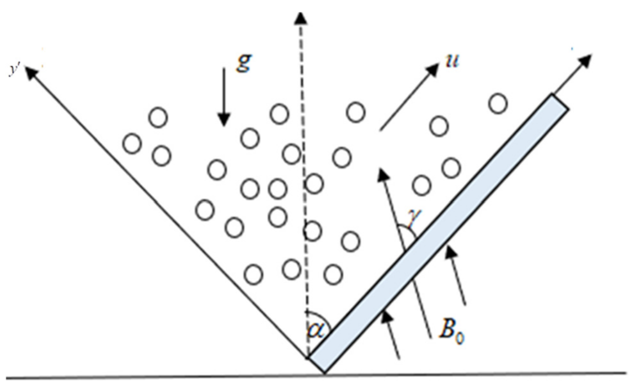

Figure 1: Geometry of the flow model.

$$v'\frac{\partial T'}{\partial y'} = \frac{k}{\rho C_p}\frac{\partial^2 T'}{\partial y'^2} + \frac{\vartheta}{C_p}\left(\frac{\partial u'}{\partial y'}\right)^2 - \frac{1}{\rho C_p}\frac{\partial q_r'}{\partial y'} + \frac{\sigma B_0^2}{\rho C_P}\sin^2\gamma u'^2 - \frac{Q_1}{\rho C_p}(T' - T_\infty'), \tag{3}$$

$$v'\frac{\partial C'}{\partial y'} = D\frac{\partial^2 C'}{\partial y'^2} - K_C(C' - C_\infty') + D_1\frac{\partial^2 T'}{\partial y'^2}. \tag{4}$$

subject to

$$\begin{aligned} &u' = 0 \quad T' = T_w,\ C' = C_w \text{ at } y' = 0,\\ &u' \to 0 \quad T' \to T'_\infty,\ C' \to C'_\infty \text{ as } y' \to \infty. \end{aligned} \tag{5}$$

Simplifying Eq. (1) gives that $v' = -v_0'$ ($v_0' > 0$), where v_0' is constant. Defining the radiative flux [13]

$$\frac{\partial q_r}{\partial y'} = 4(T' - T_\infty')\int_0^\infty K_{\lambda w}\frac{de_{b\lambda}}{dT'}d\lambda = 4I_1(T' - T'_\infty). \tag{7}$$

The following non-dimensional quantities are introduced:

$$u = \frac{u'}{v_0}, y = \frac{v_0 y'}{\vartheta}, \theta = \frac{T' - T_\infty'}{T_w - T_\infty'}, \phi = \frac{C' - C_\infty'}{C_w - C_\infty'}, \mathrm{Pr} = \frac{\mu C_p}{k},$$

$$\mathrm{Sc} = \frac{\vartheta}{D}, M = \frac{\sigma B_0^2 \vartheta}{\rho v_0^2},$$

$$\mathrm{Gr} = \frac{\vartheta g \beta_T (T_w - T_\infty')}{v_0^3}, \mathrm{Gm} = \frac{\vartheta g \beta_C (C_w - C_\infty')}{v_0^3},$$

$$E = \frac{v_0^2}{C_P(T_w - T_\infty')}, K = \frac{v_0^2 K_P}{\vartheta^2},$$

$$K_0 = \frac{\vartheta K_C}{v_0^2}, F = \frac{4I_1\vartheta^2}{k v_0^2}, Q = \frac{Q_1 v^2}{k v_0^2}, S_0 = \frac{D_1(T_w - T_\infty')}{\vartheta(C_w - C_\infty')}. \tag{8}$$

In view of the above suggested quantities, the developed system is

$$u'' + u' = -\mathrm{Gr}\cos\alpha\theta - \mathrm{Gm}\cos\alpha\phi + M_1 u, \tag{9}$$

$$\theta'' + \mathrm{Pr}\theta' - (F + Q)\theta = -\mathrm{Pr}u'^2 - \mathrm{Pr}M\sin^2\gamma u^2, \tag{10}$$

$$\phi'' + \mathrm{Sc}\phi' - \mathrm{Sc}K_0\phi = -S_0\mathrm{Sc}\theta'', \tag{11}$$

where $M_1 = M\sin^2\gamma + 1/K$.

The transformed boundary conditions are:

$$\begin{aligned} &u = 0,\ \theta = 1,\ \phi = 1 \text{ at } y = 0,\\ &u \to 0,\ \theta \to 0,\ \phi \to 0 \text{ as } y \to \infty. \end{aligned} \tag{12}$$

3 Solution of the problem

The perturbation method is imposed for solving the problem *via* analytical way. The motivations for implementation of perturbation procedure is due to fine accuracy. The initial expansion is

$$\left.\begin{aligned} u &= u_0 + Eu_1 + O(E^2),\\ \theta &= \theta_0 + E\theta_1 + O(E^2),\\ \phi &= \phi_0 + E\phi_1 + O(E^2) \end{aligned}\right\}. \tag{13}$$

Zeroth order system is

$$u_0'' + u_0' = -\mathrm{Gr}\cos\alpha\theta_0 - \mathrm{Gm}\cos\alpha\phi_0 + M_1 u_0, \tag{14}$$

$$\theta_0'' + \mathrm{Pr}\theta_0' - (F + Q)\theta_0 = 0, \tag{15}$$

$$\phi_0'' + \mathrm{Sc}\phi'_0 - \mathrm{Sc}K_0\phi_0 = -S_0\mathrm{Sc}\theta_0''. \tag{16}$$

First order expressions are

$$u_1'' + u_0' = -\mathrm{Gr}\cos\alpha\theta_1 - \mathrm{Gm}\cos\alpha\phi_1 + M_1 u_1, \tag{17}$$

$$\theta_1'' + \mathrm{Pr}\theta_1' - (F + Q)\theta_1 = -\mathrm{Pr}u_0'^2 - \mathrm{Pr}M\sin^2\gamma u_0^2, \tag{18}$$

$$\phi_1'' + \mathrm{Sc}\phi_1' - \mathrm{Sc}K_0\phi_1 = -S_0\mathrm{Sc}\phi_1'', \tag{19}$$

with

$$\begin{aligned} &u_0 = 0,\ u_1 = 0,\ \theta_0 = 1,\ \theta_1 = 0,\ \phi_0 = 1,\ \phi_1 = 0 \text{ at } y = 0\\ &u_0 \to 0,\ u_1 \to 0,\ \theta_0 \to 1,\ \theta_1 \to 0,\ \phi_0 \to 1,\\ &\phi_1 \to 0 \text{ as } y = \infty. \end{aligned} \tag{20}$$

The initial solution are

$$\theta_0 = e^{-m_1 y}, \tag{21}$$

$$\phi_0 = -A_1 e^{-m_1 y} + A_2 e^{-m_2 y}, \tag{22}$$

$$u_0 = A_3 e^{-m_1 y} - A_4 e^{-m_2 y} + A_5 e^{-m_3 y}, \tag{23}$$

$$\theta_1 = A_{18}e^{-2m_1 y} + A_{19}e^{-2m_2 y} + A_{20}e^{-2m_3 y} + A_{21}e^{-\delta_1 y} + A_{22}e^{-\delta_2 y} + A_{23}e^{-\delta_3 y} + A_{24}e^{-m_1 y}, \tag{24}$$

$$\phi_1 = A_{25}e^{-m_1 y} + A_{26}e^{-2m_1 y} + A_{27}e^{-2m_2 y} + A_{28}e^{-2m_3 y} + A_{29}e^{-\delta_1 y} + A_{30}e^{-\delta_2 y} + A_{31}e^{-\delta_3 y} + A_{32}e^{-m_2 y}, \tag{25}$$

$$u_1 = A_{33}e^{-m_1y} + A_{34}e^{-m_2y} + A_{35}e^{-2m_1y} + A_{36}e^{-2m_2y} + A_{37}e^{-2m_3y} + A_{38}e^{-\delta_1y} + A_{39}e^{-\delta_2y} + A_{40}e^{-\delta_3y} + A_{41}e^{-m_3y}. \quad (26)$$

The requested solution is

$$u = A_3e^{-m_1y} - A_4e^{-m_2y} + A_5e^{-m_3y} + E[A_{33}e^{-m_1y} + A_{34}e^{-m_2y} + A_{35}e^{-2m_1y} + A_{36}e^{-2m_2y} + A_{37}e^{-2m_3y} + A_{38}e^{-\delta_1y} + A_{39}e^{-\delta_2y} + A_{40}e^{-\delta_3y} + A_{41}e^{-m_3y}]. \quad (27)$$

$$\theta = e^{-m_1y} + E[A_{18}e^{-2m_1y} + A_{19}e^{-2m_2y} + A_{20}e^{-2m_3y} + A_{21}e^{-\delta_1y} + A_{22}e^{-\delta_2y} + A_{23}e^{-\delta_3y} + A_{24}e^{-m_1y}], \quad (28)$$

$$\phi = -A_1e^{-m_1y} + A_2e^{-m_2y} + E[A_{25}e^{-m_1y} + A_{26}e^{-2m_1y} + A_{27}e^{-2m_2y} + A_{28}e^{-2m_3y} + A_{29}e^{-\delta_1y} + A_{30}e^{-\delta_2y} + A_{31}e^{-\delta_3y} + A_{32}e^{-m_2y}]. \quad (29)$$

Defining the surface skin force [3]

$$\tau = \left(\frac{\partial u}{\partial y}\right)_{y=0},$$

$$\tau = [-m_3A_5 + m_2A_4 - m_1A_3] + E[m_1A_{33} - m_2A_{34} - 2m_1A_{35} - 2m_2A_{36} - 2m_3A_{37} - \delta_1A_{38} - \delta_2A_{39} - \delta_3A_{40} - m_3A_{41}]. \quad (30)$$

The Nusselt number is expressed as [3]

$$\mathrm{Nu} = -\left(\frac{\partial\theta}{\partial y}\right)_{y=0},$$

$$\mathrm{Nu} = m_1 + E[m_1A_{24} + 2m_1A_{18} + 2m_2A_{19} + 2m_3A_{20} + \delta_1A_{21} + \delta_2A_{22} + \delta_3A_{23}]. \quad (31)$$

Defining the Sherwood number [3]

$$\mathrm{Sh} = -\left(\frac{\partial\phi}{\partial y}\right)_{y=0},$$

$$\mathrm{Sh} = [m_2A_2 - m_1A_1] + E[m_1A_{25} + 2m_1A_{26} + 2m_2A_{27} + 2m_3A_{28} + \delta_1A_{29} + \delta_2A_{30} + \delta_3A_{31} + m_2A_{32}]. \quad (32)$$

4 Results and discussion

The physical significance of parameters for velocity profile u, temperature θ, and concentration ϕ is visualized in this section. The results and observations are supported with graphs. Figure 2(a)–(c) pronounced the variation in velocity u subject to variation in permeability parameter K, magnetic parameter M, and inclined angle γ. The analysis is subject to two regimes of plate like cooler and heated surface. Figure 2(a) shows the assessment of u for permeability parameter K. A boosted effect in determination of u is noticed for K. Such effects are physically justified due to permeability of porous regime. Figure 2(b) addresses the onset of magnetic parameter M on u. More slower rate of velocity has been exhibited for M in both heated and cooler surface. Such decrement appearing in u is due to Lorentz force which exclusively presents resistivity in motion. Figure 2(c) justified the fluctuated pattern in the behavior of u against inclination angle γ. A control of the changing u due to γ is observed for both surface constraints. Figure 3(a) and (b) addresses the prediction for u due to Grashof number (Gr) and Mass Grashof number (Gm). Both parameters are physically involved in the role of buoyancy forces. An increment is presented in change of u for both parameters.

Figure 4(a) and (b) is prepared in order to justify the aim of Prandtl number Pr on temperature profile θ. The decreasing analysis in the rate of θ is predicted for Pr. Physically, the slower rate of heat transfer is pronounced for less thermal diffusivity. Figure 5(a) and (b) expresses the contribution of γ on θ. The decreasing change is exhibited in θ for increasing γ. The decreasing change is more progressive for cooler surface. The analysis for observing fluctuation in θ due to heat absorption parameter Q is shown in Figure 6(a) and (b). The slower heat fluctuation is inspected when heat absorption phenomenon appears. The removal of heat transfer results in a slower temperature profile of both cooler and heated plates. Figure 7(a) and (b) shows the change in concentration field ϕ due to Soret number S_0. An improvement in concentration is noticed for S_0. Figure 8(a) and (b) shows the contribution of reaction parameter K_0 in the field of ϕ. Decreasing outcomes are observed for ϕ due to K_0.

Table 1 presents the variation in wall shear force due to different parameters like Gm, M, and K. The analysis is subject to various values of Prandtl number. Note that these values are associated with different liquids like mercury, electrolytic solution, air, and water. A peak variation in wall shear force is noted when Gm is maximum. The increasing change is more reflective for mercury. Similar effects are noted for K. Tables 2 and 3 present the variation in involved parameters for Nusselt number and Sherwood number, respectively. The analysis is subject to prediction of decomposition of mercury, electrolytic solution, air, and water.

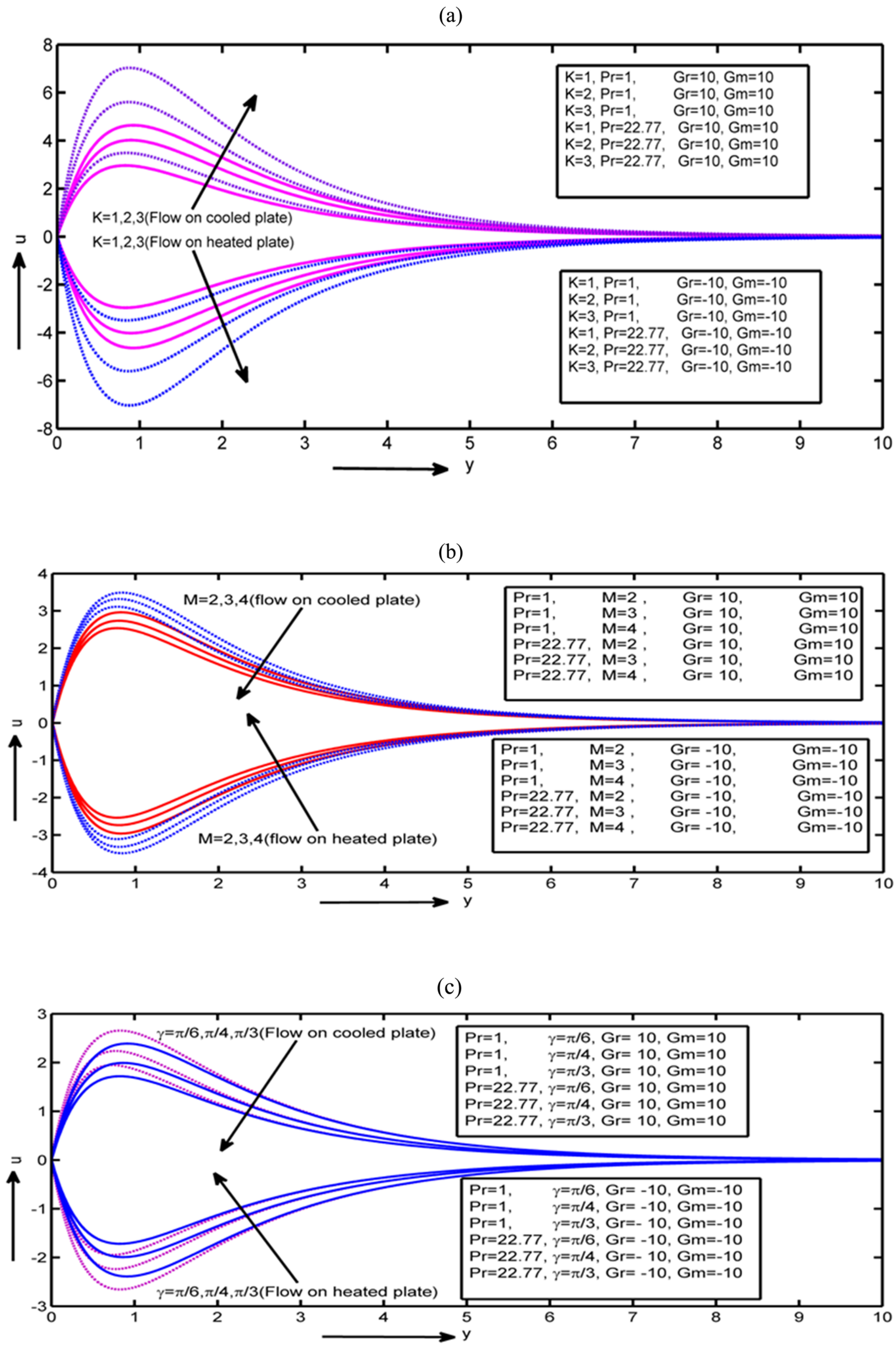

Figure 2: Velocity profile for (a) K, (b) M, and (c) γ.

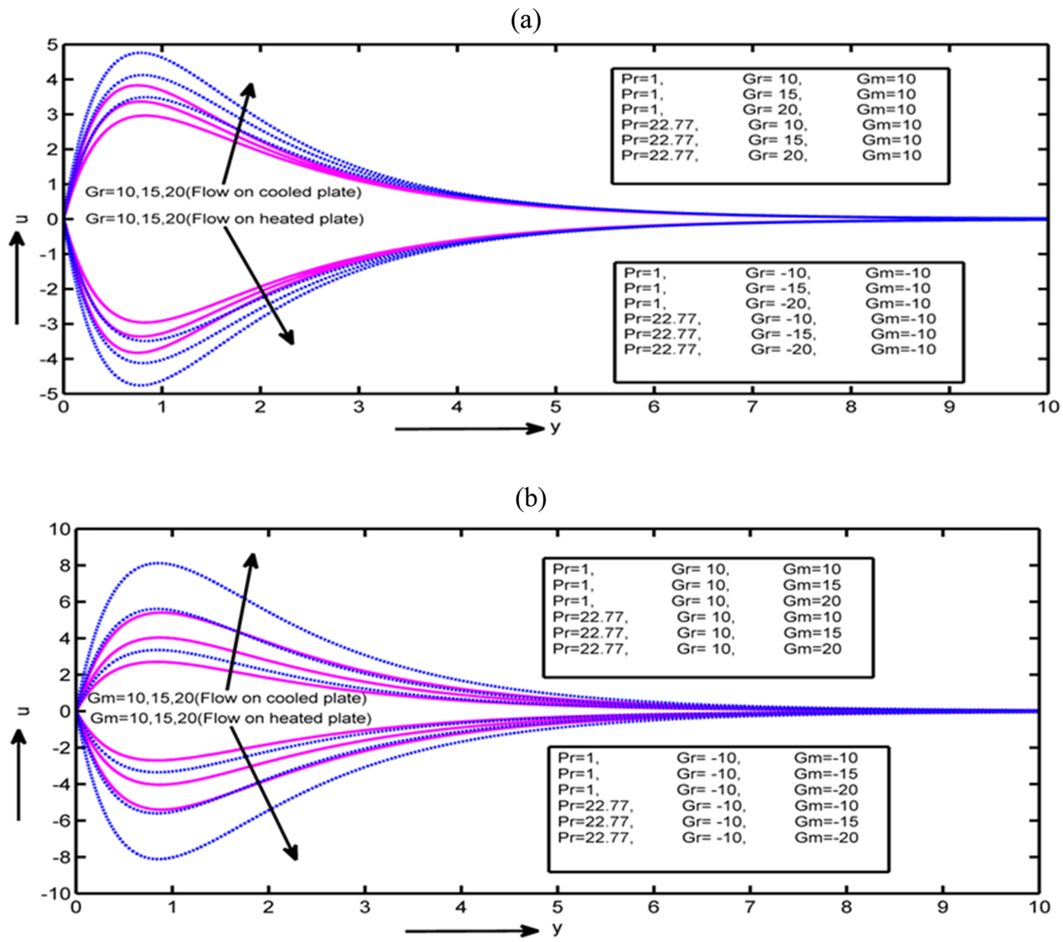

Figure 3: Velocity profile for (a) Gr and (b) Gm.

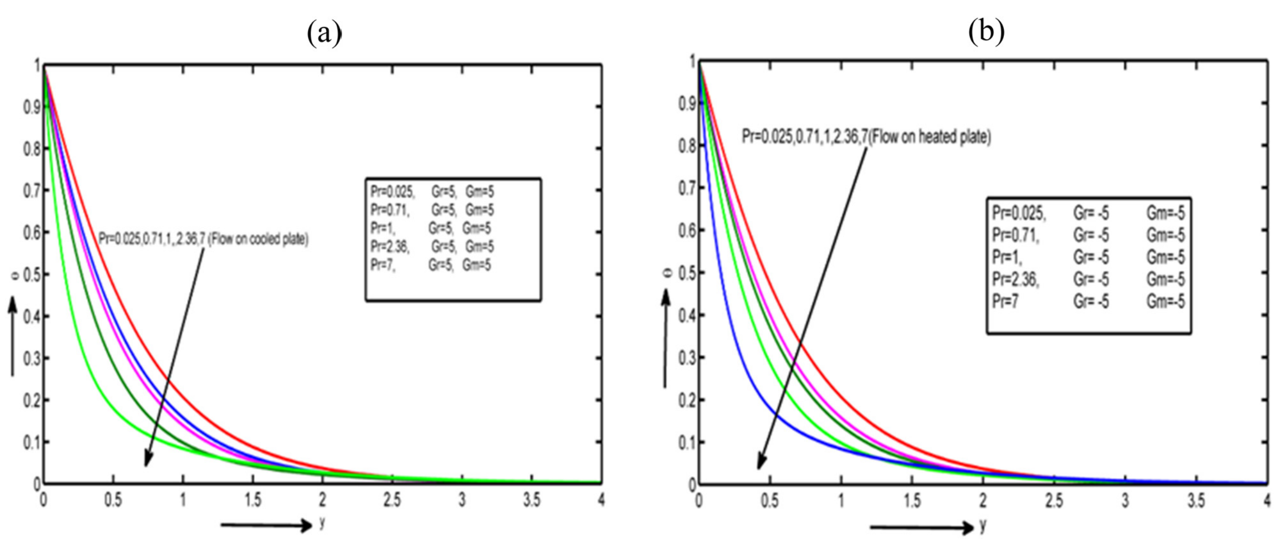

Figure 4: Variation in temperature profile due to Pr: (a) flow on cooled plate and (b) flow on heated plate.

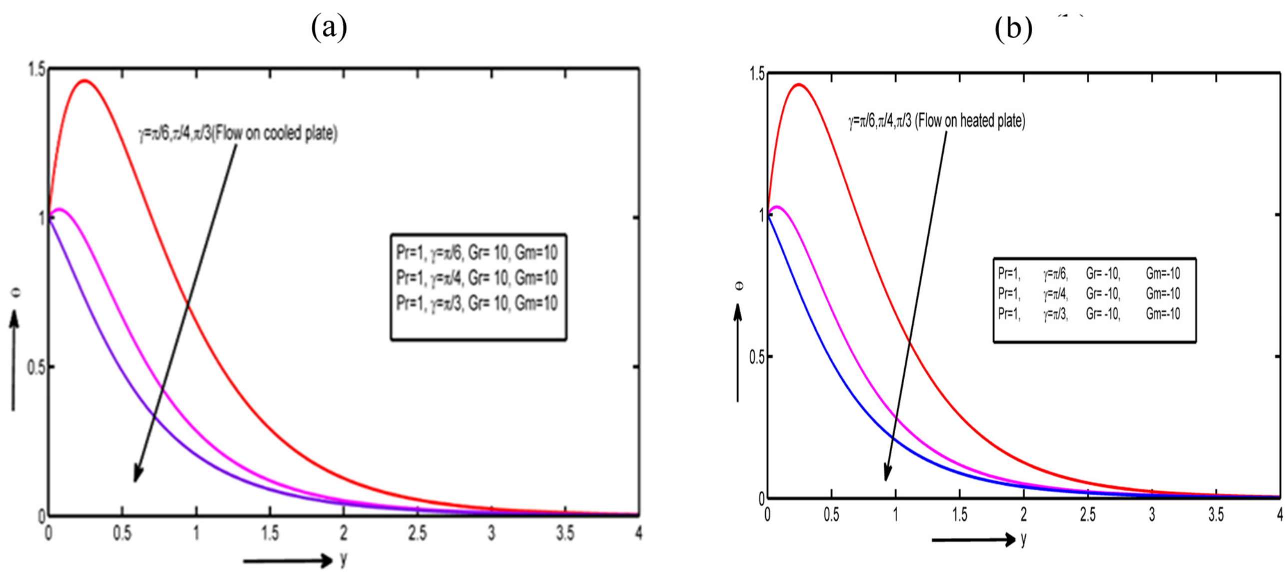

Figure 5: Variation in temperature profile due to γ: (a) flow on cooled plate and (b) flow on heated plate.

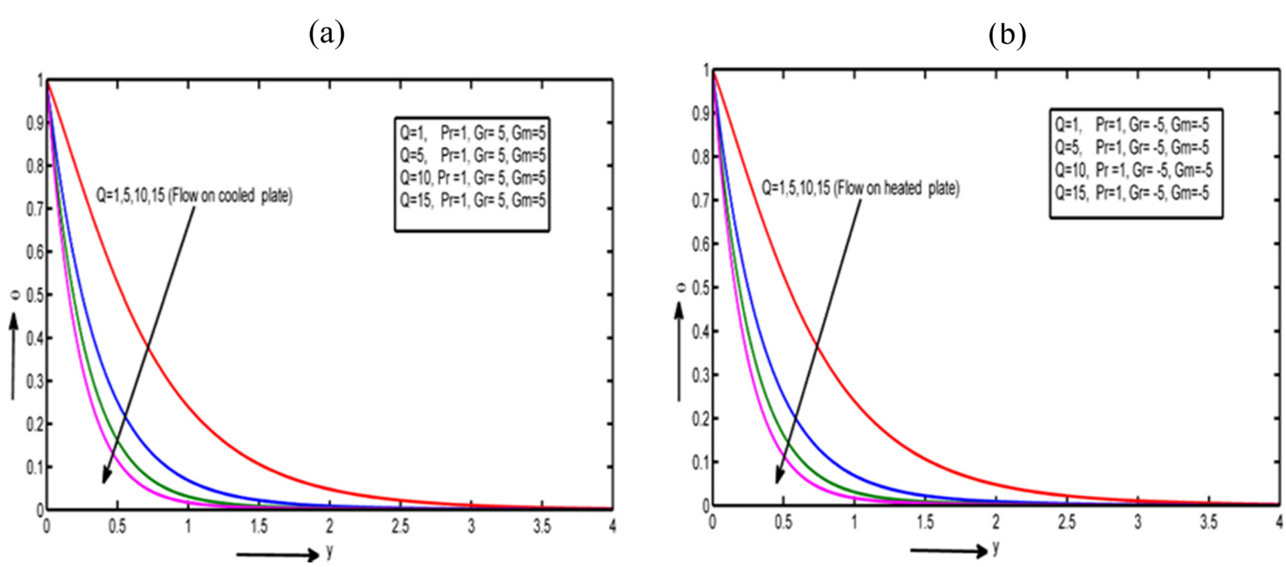

Figure 6: Variation in temperature profile due to Q: (a) flow on cooled plate and (b) flow on heated plate.

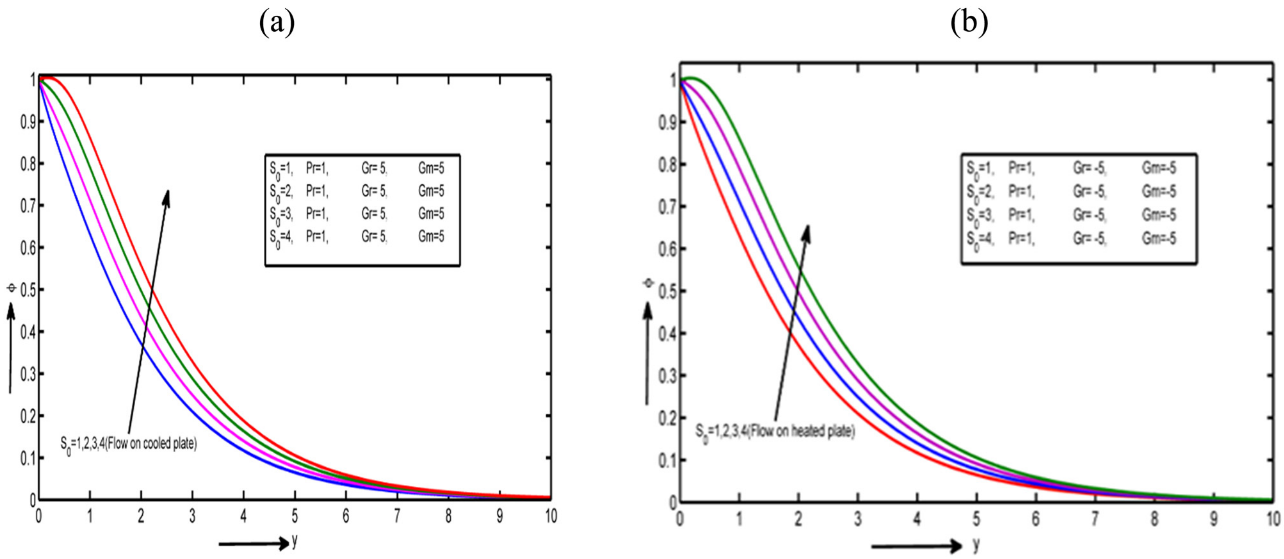

Figure 7: Variation in concentration profile due to S_0: (a) flow on cooled plate and (b) flow on heated plate.

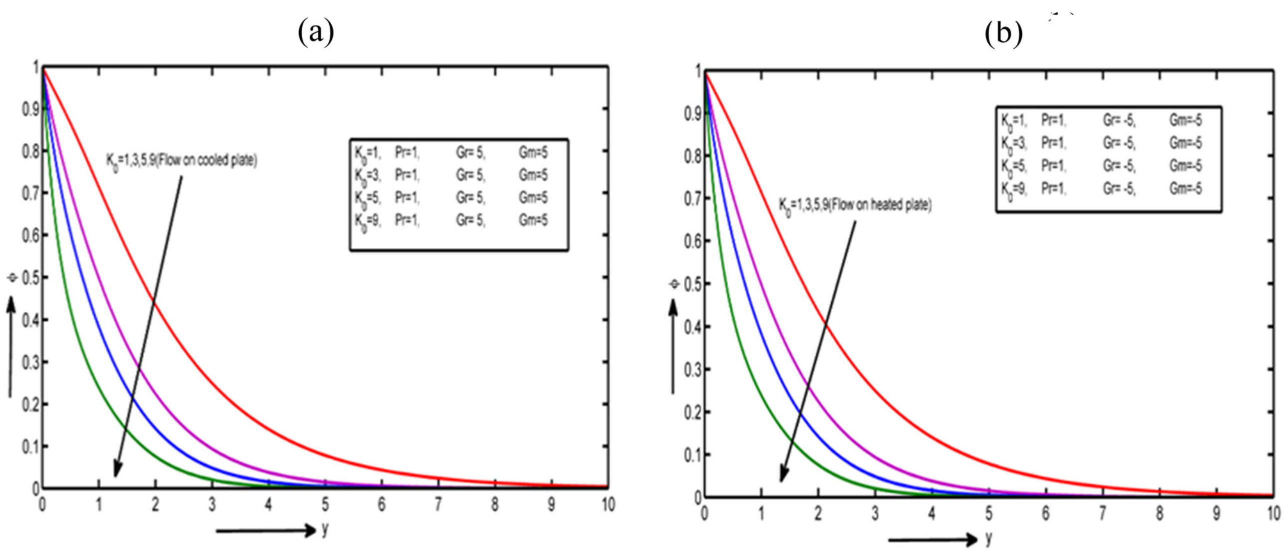

Figure 8: Variation in concentration profile due to K_0: (a) flow on cooled plate and (b) flow on heated plate.

Table 1: Numerical change in wall shear force due to different parameters

Gm	M	K	Wall shear force			
			Mercury (Pr=0.025)	Electrolytic solution (Pr=1.0)	Air (Pr=0.71)	Water (Pr=7.0)
5.0			6.6185	6.3490	7.3516	5.6751
10			10.5656	10.4235	12.1723	10.2210
15			14.5238	14.5136	17.0227	14.7317
	2.0		6.5075	6.3490	7.3516	5.6751
	3.0		5.7299	5.5649	6.1709	4.9709
	4.0		5.7984	5.9447	7.4704	5.4962
		2.0	7.0617	7.0966	6.9600	6.2316
		3.0	7.2847	7.6694	7.2098	6.4633
		4.0	7.4052	8.2918	7.3516	6.5907

Table 2: Variations in Nusselt number for different parameters

S_0	F	Q	Nusselt number			
			Mercury (Pr=0.025)	Electrolytic solution (Pr=1.0)	Air (Pr=0.71)	Water (Pr=7.0)
1			1.4091	1.5740	1.6245	6.1734
2			1.4098	1.6582	1.6152	5.7578
3			1.4099	1.6925	1.6071	5.2751
	4		1.8510	2.6302	2.4460	6.7311
	6		2.6516	3.0822	2.9409	7.0466
		3	1.9850	2.2331	0.6403	6.5589
		5	2.4299	2.8740	2.7269	6.8932
		6	2.6516	3.0822	2.9409	7.0466

Table 3: Variations in Sherwood number for different parameters

Sc	K_0	S_0	Sherwood number			
			Mercury (Pr=0.025)	Electrolytic solution (Pr=1.0)	Air (Pr=0.71)	Water (Pr=7.0)
0.22			0.4054	0.3667	0.3608	−0.6481
0.30			0.4959	0.4202	0.4265	−0.9395
0.60			0.9047	0.6327	0.7222	−1.8236
	0.5		0.2469	0.2182	0.2080	−0.7642
	1.5		0.5289	0.4830	0.4803	−0.5474
	3		0.8116	0.7498	0.7542	−0.2979
		2	0.2188	0.1046	0.1250	−1.7067
		4	−0.1539	−0.4007	−0.3128	−3.1048
		6	−0.5231	−0.6650	−0.6241	−3.2517

5 Conclusion

The study investigates the heat and mass transfer in mixed convection flow over a porous inclined plate. A perturbation solution is derived in a closed form. The analysis reveals that the velocity profile is influenced by the Grashof number, leading to an increase in velocity. Changes in the inclined angle result in a decrease in the velocity magnitude. Heat transfer is found to decrease with the Prandtl number, with a more pronounced effect on the heated surface. Slower heat transfer is observed due to heat absorption. The concentration field is affected by the Soret number, with a greater impact on the cooler surface. A decrease in the concentration profile is noted. The skin friction coefficient increases with the Grashof number for mercury, electrolytic solution, air, and water decomposition.

Acknowledgments: The authors are thankful to the Deanship of Graduate Studies and Scientific Research at University of Bisha for supporting this work through the Fast-Track Research Support Program. The authors express their gratitude to Princess Nourah bint Abdulrahman University Researchers Supporting Project number (PNURSP2024R453), Princess Nourah bint Abdulrahman University, Riyadh, Saudi Arabia.

Funding information: The University of Bisha for supporting this work through the fast-track research support program. The authors express their gratitude to Princess Nourah bint Abdulrahman University Researchers Supporting Project number (PNURSP2024R453), Princess Nourah bint Abdulrahman University, Riyadh, Saudi Arabia.

Author contributions: All authors have accepted responsibility for the entire content of this manuscript and approved its submission.

Conflict of interest: The authors state no conflict of interest.

References

[1] Chamkha AJ. Thermal radiation and buoyancy effects on hydromagnetic flow over an accelerating permeable surface with heat source or sink. Int J Eng Sci. 2000;38(15):1699–712.

[2] Pal D, Mondal H. Effects of Soret Dufour, chemical reaction and thermal radiation on MHD non-Darcy unsteady mixed convective heat and mass transfer over a stretching sheet. Commun Nonlinear Sci Numer Simul. 2011;16(4):1942–58.

[3] Obulesu M, Charankumar G, Bhagyashree M, Lorenzini G. MHD heat and mass transfer steady flow of aconvective fluid through a

porous plate in the preseance of multiple parameters. J Adv Res Fluid Mech Therm Sci. 2022;89:56–75.
[4] Mahmoud MAA. Thermal radiation effect on unsteady MHD free convection flow past a vertical plate with temperature-dependent viscosity. Can J Chem Eng. 2009;87(1):47–52.
[5] Turkyilmazoglu M. The analytical solution of mixed convection heat transfer and fluid flow of a MHD viscoelastic fluid over a permeable stretching surface. Int J Mech Sci. 2013;77:263–8.
[6] Nandalur AA. Hall current impacts on unsteady MHD free convective flow past an infinite vertical porous surface. Heat Transf. 2021;50(5):4656–68.
[7] Khan M, Hussain M, Azam M. Magnetohydrodynamic flow of Carreau fluid over a convectively heated surface in the presence of thermal radiation. J Magn Magn Mater. 2016;412:63–8.
[8] Mansour MA, Rashad AM, Mallikarjuna B, Hussein AK, Aichouni M, Kolsi L. MHD mixed bioconvection in a square porous cavity filled by gyrotactic microorganisms. Int J Heat Technol. June, 2019;37(2):433–45.
[9] Kumar R, Bhattacharyya A, Seth GS, Chamkha AJ. Transportation of magnetite nanofluid flow and heat transfer over a rotating porous disk with Arrhenius activation energy: fourth order Noumerov's method. Chin J Phys. 2021;69:172–85.
[10] Lou Q, Ali B, Rehman SU, Habib D, Abdal S, Shah NA, et al. Micropolar dusty fluid: Coriolis force effects on dynamics of MHD rotating fluid when lorentz force is significant. Mathematics. 2022;10(15):2630.
[11] Ashraf MZ, Rehman SU, Farid S, Hussein AK, Ali B, Shah NA, et al. Insight into significance of bioconvection on MHD tangent hyperbolic nanofluid flow of irregular thickness across a slender elastic surface. Mathematics. 2022;10:2592.
[12] Ma H, He B, Su L, He D. Heat transfer enhancement of nanofluid flow at the entry region of microtubes. Int J Therm Sci. February 2023;184:107944.
[13] Prabhakar Reddy B, Jefta Sunzu P. Thermal radiation and viscous dissipation effects on MHD heat and mass difussion flow past a surface embedded in a porous medium with chemical reaction. Int J Math Appl. 2016;4(2):91–103.
[14] Rashidi MM, Rostami B, Freidoonimehr N, Abbasbandy S. Free convective heat and mass transfer for MHD fluid flow over a permeable vertical stretching sheet in the presence of the radiation and buoyancy effects. Ain Shams Eng J. 2014;5(3):901–12.
[15] Shankar Goud B, Dharmendar Reddy Y. Chemical reaction and Soret effect on an unsteady MHD heat and mass transfer fluid flow along an infinite vertical plate with radiation and heat absorption. J Indian Chem Soc. November 2022;99(11):100762. doi: 10.1016/j.jics.2022.100762.
[16] Seid E, Haile E, Walelign T. Multiple slip, Soret and Dufour effects in fluid flow near a vertical stretching sheet in the presence of magnetic nanoparticles. Int J Thermofluids. 2022;13:100136.
[17] Rauf A, Hussain F, Mushtaq A, Shah NA, Ali MR. MHD mixed convection flow for Maxwell hybrid nanofluid with Soret, Dufour and Morphology effects. Arab J Chem. 2023;16(8):104965.
[18] Siddique I, Nadeem M, Awrejcewicz J, Pawłowski W. Soret and Dufour effects on unsteady MHD second-grade nanofluid flow across an exponentially stretching surface. Sci Rep. 2022;12(1):11811.
[19] Li S, Imtiaz M, Khan MI, Kumar RI, Akramova KS. Applications of Soret and Dufour effects for Maxwell nanomaterial by convectively heated surface. Numer Heat Transf A: Appl. 2024. doi: 10.1080/10407782.2024.2314224. In press.
[20] Farooq S, Khan MI, Riahi A, Chammam W, Khan WA. Modeling and interpretation of peristaltic transport in single wall carbon nanotube flow with entropy optimization and Newtonian heating. Comput Methods Prog Biomed. 2020;192:105435.
[21] Li S, Khan MI, Khan SU, Abdullaev S, Habibullah, Mohamed MMI, et al. Effectiveness of melting phenomenon in two phase dusty carbon nanotubes (nanomaterials) flow of Eyring-Powell fluid: Heat transfer analysis. Chin J Phys. 2023. doi: 10.1016/j.cjph.2023.09.013.
[22] Khan MI, Waqas H, Farooq U, Khan SU, Chu YM, Kadry S. Assessment of bioconvection in magnetized Sutterby nanofluid configured by a rotating disk: A numerical approach. Mod Phys Lett B. 2021;35:2150202.
[23] Li S, Rajashekhar C, Nisar KS, Mebarek-Oudina F, Vaidya H, Khan MI, et al. Peristaltic transport of a Ree-Eyring fluid with non-uniform complaint channel: An analysis through varying conditions. ZAMM-J Appl Math Mech/Z für Angew Math Mech. 2024;104(2):e202300073. doi: 10.1002/zamm.202300073.
[24] Wang N, Li X, Lian X, Zhuang Q, Wang J, Li J, et al. Acetate ions facilitated immobilization of highly dispersed transition metal oxide nanoclusters in mesoporous silica. Inorg Chem. 2024;63(9):4393–403. doi: 10.1021/acs.inorgchem.4c00024.
[25] Cao A, Hua Y, Sun Z, Meng Z, Guo Z, Zhang N. Study on reduction of pressure oscillation in low-velocity steam jet condensation. Ann Nucl Energy. 2024;197:110271.
[26] Dai H, Liu Y, Guadagnini A, Yuan S, Yang J, Ye M. Comparative assessment of two global sensitivity approaches considering model and parameter uncertainty. Water Resour Res. 2024;60(2):e2023WR036096.
[27] Xiao D, Liu M, Li L, Cai X, Qin S, Gao R, et al. Model for economic evaluation of closed-loop geothermal systems based on net present value. Appl Therm Eng. 2023;231:121008.
[28] Bhatti MM, Shahid A, Sarris IE, Anwar Bég O. Spectral relaxation computation of Maxwell fluid flow from a stretching surface with quadratic convection and non-Fourier heat flux using Lie symmetry transformations. Int J Mod Phys B. 2023;37(9):2350082.
[29] Li S, Khan MI, Ali F, Abdullaev SS, Saadaoui S, Habibullah. Mathematical modeling of mixed convective MHD Falkner-Skan squeezed Sutterby multiphase flow with non-Fourier heat flux theory and porosity. Appl Math Mech-Engl Ed. 2023;44:2005–18.
[30] Li S, Abbas T, Al-Khaled K, Khan SU, Ul Haq E, Abdullaev SS, et al. Insight into the heat transfer across the dynamics of Burger fluid due to stretching and buoyancy forces when thermal radiation and heat source are significant. Pramana J Phys. 2023;97:196.
[31] Li S, Safdar M, Taj S, Bilal M, Ahmed S, Khan MI, et al. Generalized Lie similarity transformations for the unsteady flow and heat transfer under the influence of internal heating and thermal radiation. Pramana J Phys. 2023;97:203.
[32] Li S, Abbasi A, Farooq W, Gul M, Khan MI, Nafasova G, et al. Heat and mass transfer characteristics of Al_2O_3/H_2O and $(Al_2O_3+Ag)/H_2O$ nanofluids adjacent to a solid sphere: A theoretical study. 2024. doi: 10.1080/10407782.2024.2306177. In press.
[33] Yu H, Wang H, Lian Z. An assessment of seal ability of tubing threaded connections: A hybrid empirical-numerical method. J Energy Resour Technol. 2022;145(5):052902. doi: 10.1115/1.4056332.
[34] Yang S, Zhang Y, Sha Z, Huang Z, Wang H, Wang F, et al. Deterministic manipulation of heat flow *via* three-dimensional-printed thermal meta-materials for multiple protection of critical components. ACS Appl Mater Interfaces. 2022;14(34):39354–63.
[35] Zhu S, Li X, Bian Y, Dai N, Yong J, Hu Y, et al. Inclination-enabled generalized microfluid rectifiers *via* anisotropic slippery hollow tracks. Adv Mater Technol. 2023;8(16):2300267.
[36] Sun L, Liang T, Zhang C, Chen J. The rheological performance of shear-thickening fluids based on carbon fiber and silica nanocomposite. Phys Fluids. 2023;35(3):32002.
[37] Kong L, Liu Y, Dong L, Zhang L, Qiao L, Wang W, et al. Enhanced red luminescence in $CaAl_{12}O_{19}$: Mn^{4+} *via* doping Ga^{3+} for plant growth lighting. Dalton Trans. 2020;49(6):1947–54.

Appendix

$$M_1 = M\sin^2\gamma + \frac{1}{K} \quad M_2 = F + Q,$$

$$m_1 = \frac{\mathrm{Pr} + \sqrt{\mathrm{Pr}^2 + 4M_2}}{2}$$

$$m_2 = \frac{\mathrm{Sc} + \sqrt{\mathrm{Sc}^2 + 4K_0\mathrm{Sc}}}{2}$$

$$m_3 = \frac{1 + \sqrt{1 + 4M_1}}{2}$$

$$A_1 = \frac{m_1^2 S_0\mathrm{Sc}}{m_1^2 - \mathrm{Sc}m_1 - K_0\mathrm{Sc}}$$

$$A_2 = 1 + A_1$$

$$A_3 = \frac{A_1\mathrm{Gm}\ \cos\alpha - \mathrm{Gr}\ \cos\alpha}{m_1^2 - m_1 - M_1}$$

$$A_4 = \frac{A_2\mathrm{Gm}\cos\alpha}{m_2^2 - m_2 - M_1} A_5 = A_4 - A_3$$

$$\lambda_1 = m_1A_3 \quad \lambda_2 = m_2A_4 \quad \lambda_3 = m_3A_5$$

$$A_6 = \frac{-\mathrm{Pr}\lambda_1^2}{4m_1^2 - 2\ Prm_1 - M_2}$$

$$A_7 = \frac{-\mathrm{Pr}\lambda_2^2}{4m_2^2 - 2Prm_2 - M_2}$$

$$A_8 = \frac{-\mathrm{Pr}\lambda_3^2}{4m_3^2 - 2Prm_3 - M_2}$$

$$\delta_1 = m_1 + m_2$$

$$\delta_2 = m_2 + m_3$$

$$\delta_3 = m_3 + m_1$$

$$A_9 = \frac{2\lambda_1\lambda_2\mathrm{Pr}}{\delta_1^2 - \mathrm{Pr}\delta_1 - M_2} \quad A_{10} = \frac{2\lambda_2\lambda_3\mathrm{Pr}}{\delta_2^2 - \mathrm{Pr}\delta_2 - M_2}$$

$$A_{11} = \frac{-2\lambda_1\lambda_3\mathrm{Pr}}{\delta_3^2 - \mathrm{Pr}\delta_3 - M_2} \quad A_{12} = \frac{-\mathrm{Pr}M\ \sin^2\gamma A_3^2}{4m_1^2 - 2\mathrm{Pr}m_1 - M_2}$$

$$A_{13} = \frac{-\mathrm{Pr}M\ \sin^2\gamma A_4^2}{4m_2^2 - 2\mathrm{Pr}m_2 - M_2}$$

$$A_{14} = \frac{-\mathrm{Pr}M\ \sin^2\gamma A_5^2}{4m_3^2 - 2\mathrm{Pr}m_3 - M_2}$$

$$A_{15} = \frac{2A_3A_4\mathrm{Pr}M\sin^2\gamma}{\delta_1^2 - \mathrm{Pr}\delta_1 - M_2} \quad A_{16} = \frac{2A_4A_5\mathrm{Pr}M\sin^2\gamma}{\delta_2^2 - \mathrm{Pr}\delta_2 - M_2}$$

$$A_{17} = \frac{-2A_5A_3\mathrm{Pr}M\sin^2\gamma}{\delta_3^2 - \mathrm{Pr}\delta_3 - M_2} \quad A_{18} = A_6 + A_{12} \quad A_{19} = A_7 + A_{13}$$

$$A_{20} = A_8 + A_{14} \quad A_{21} = A_9 + A_{15} \quad A_{22} = A_{10} + A_{16}$$

$$A_{23} = A_{11} + A_{17} \quad A_{24} = -(A_{18} + A_{19} + A_{20} + A_{21} + A_{22} + A_{23})$$

$$A_{25} = \frac{-m_1^2A_{24}S_0\mathrm{Sc}}{m_1^2 - \mathrm{Sc}m_1 - K_0\mathrm{Sc}} \quad A_{26} = \frac{-4m_1^2A_{18}S_0\mathrm{Sc}}{4m_1^2 - 2\mathrm{Sc}m_1 - K_0\mathrm{Sc}}$$

$$A_{27} = \frac{-4m_2^2A_{19}S_0\mathrm{Sc}}{4m_2^2 - 2\mathrm{Sc}m_2 - K_0\mathrm{Sc}} \quad A_{28} = \frac{-4m_3^2A_{20}S_0\mathrm{Sc}}{4m_3^2 - 2\mathrm{Sc}m_3 - K_0\mathrm{Sc}}$$

$$A_{29} = \frac{-\delta_1^2A_{21}S_0\mathrm{Sc}}{\delta_1^2 - \mathrm{Sc}\delta_1 - \mathrm{Sc}K_0} \quad A_{30} = \frac{-\delta_2^2A_{22}S_0\mathrm{Sc}}{\delta_2^2 - \mathrm{Sc}\delta_2 - \mathrm{Sc}K_0}$$

$$A_{31} = \frac{-\delta_3^2A_{23}S_0\mathrm{Sc}}{\delta_3^2 - \mathrm{Sc}\delta_3 - \mathrm{Sc}K_0}$$

$$A_{32} = -(A_{25} + A_{26} + A_{27} + A_{28} + A_{29} + A_{30} + A_{31})$$

$$A_{33} = \frac{-A_{24}\mathrm{Gr}\cos\alpha - A_{25}\mathrm{Gm}\cos\alpha}{m_1^2 - m_1 - M_1} \quad A_{34} = \frac{-A_{32}\mathrm{Gm}\cos\alpha}{m_2^2 - m_2 - M_1}$$

$$A_{35} = \frac{-A_{18}\mathrm{Gr}\cos\alpha - A_{26}\mathrm{Gm}\cos\alpha}{4m_1^2 - 2m_1 - M_1}$$

$$A_{36} = \frac{-A_{19}\mathrm{Gr}\cos\alpha - A_{27}\mathrm{Gm}\cos\alpha}{4m_2^2 - 2m_2 - M_1}$$

$$A_{37} = \frac{-A_{20}\mathrm{Gr}\cos\alpha - A_{28}\mathrm{Gm}\cos\alpha}{4m_3^2 - 2m_3 - M_1}$$

$$A_{38} = \frac{-A_{21}\mathrm{Gr}\cos\alpha - A_{29}\mathrm{Gm}\cos\alpha}{\delta_1^2 - \delta_1 - M_1}$$

$$A_{39} = \frac{-A_{22}\mathrm{Gr}\cos\alpha - A_{30}\mathrm{Gm}\cos\alpha}{\delta_2^2 - \delta_2 - M_1}$$

$$A_{40} = \frac{-A_{23}\mathrm{Gr}\cos\alpha - A_{31}\mathrm{Gm}\cos\alpha}{\delta_3^2 - \delta_3 - M_1}$$

$$A_{41} = -(A_{33} + A_{34} + A_{35} + A_{36} + A_{37} + A_{38} + A_{39} + A_{40}).$$